Desalination and Water Treatment
www.deswater.com

doi: 10.5004/dwt.2019.23915

151 (2019) 199–211
May

Adsorption, kinetic and thermodynamic studies of safranin and methylene blue on a novel adsorbent based on phosphorylated sawdust

Mosaed S. Alhumaimess

Chemistry Department, College of Science, Jouf University, PO Box 2014, Sakaka, Saudi Arabia, Tel. +966 553399656; email: mosaed@ju.edu.sa

Received 13 August 2018; Accepted 4 February 2019

ABSTRACT

The effectiveness of phosphorylated sawdust (RSD@P) for the adsorption of both safranin and methylene blue from aqueous systems has been studied. The related adsorption factors; pH, stirring time, initial dye concentrations and amount of RSD@P have been demonstrated. The adsorption's dependence on temperature, adsorption kinetic and adsorption isotherms were studied. The pseudo-second-order model was more significant (R^2 = 0.99) for describing the adsorption kinetic of both dyes than the pseudo-first-order and Elovich ones. The adsorption process best fitted the Langmuir isotherm model (R^2 = 0.99) rather than the other studied models. The calculated adsorption capacities using the Langmuir model were 109.22, 124.72, 135.9 mgg^{-1} for safranin and 123.46, 138.89, 158.73 mgg^{-1} for methylene blue at 293, 303 and 318 K, respectively. Thermodynamic studies emphasized that the adsorption process was spontaneous, endothermic and physical in nature (ΔH^o = 12. 48, 12. 83 $kj.mol^{-1}$ for safranin and methylene blue, respectively). The results showed the elevation removal of dyes by @P rather than that obtained by raw sawdust using the same dosage (0.01 g) and experimental conditions. Thus, RSD@P can serve as a promising adsorbent for the removal of safranin and methylene blue from aqueous solutions.

Keywords: Phosphorylated sawdust; Adsorption; Safranin; Methylene blue; Kinetic; Thermodynamics

1. Introduction

The treatment of water contamination due to colored materials has been of great concern for many studies. Dyes and pigments as colored materials are principally employed in the plastics, paper, food, and pharmaceutical industries. These colored materials, on reaching surface and ground water sources, can cause aesthetic pollution and poison aquatic life [1,2]. Safranin and methylene blue are water-soluble organic cationic dyes that have been used in several industries. Safranin is widely applied to certain food products as flavor and color additives. It is also applied to dyeing processes in textile industries [3,4]. The deleterious effect of safranin's presence in water can cause serious harm to human health including irritation and burning to the mouth, eye and skin. Its arrival in the digestive system causes pain, nausea, vomiting and diarrhea [3,5]. Methylene blue has been utilized in the paper, textile, leather, and cosmetic industries [6,7]. Pollution from methylene blue leads to eyesight, respiratory and abdominal disorders [8]. Most dyes have a synthetic origin and a complex structure, so they are very stable against heat, biodegradation and breakdown by chemicals [9]. These properties make their removal from aqueous systems hard to some extent. Recently, their discharge from wastewater using several techniques has been investigated [10–14]. Adsorption is the most physiochemical treatment technique that has been widely used because of its economic viability, effective dye treatment and sludge free clean operation [15]. Nowadays, several adsorbent materials have been reported for dye removal such as calcined mussel shells [16], chitosan [17], raw kaolin [18], magnetic mesoporous clay [19], carboxylated cellulose derivative [20],

biomass fly ash geopolymer [8], oil-free algal biomass [21] etc. The main objective of this work is to attempt to adsorb these dyes using a new adsorbed material and to study the related adsorption models in full. On the basis of finding a new low-cost and eco-friendly adsorbent, our group recently modified wood sawdust by phosphorylating the hydroxyl groups using phosphorous oxychloride. The obtained adsorbent (RSD@P) successfully increased the efficiency of heavy metal removal compared with the raw material [22]. The promising results of the current adsorbent regarding some heavy metal uptake were a major reason for its trial and exploitation for the adsorption of safranin and methylene blue removal from aqueous solutions. Every factor affecting the dye's adsorption, including pH, stirring time, initial dye concentration, amount of RSD@P and temperature, has been demonstrated. Five adsorption isotherm models, four kinetic models, and thermodynamic and desorption studies have been included in this study. Therefore, the successful use of this adsorbent for the uptake of such large dye molecules will be another crucial environmental application besides its heavy metal adsorption ability.

2. Materials and methods

2.1. Chemicals

Safranin ($C_{20}H_{19}ClN_4$, Mol. wt. = 350.8) and methylene blue, MB ($C_{16}H_{18}N_3SCl$, Mol. wt. = 319.85) (Fig. 1) were purchased from Merck, Germany.

Sodium hydroxide, acetic acid, nitric acid and hydrochloric acid were obtained from BDH, England. The phosphorus oxychloride ($POCl_3$), Triethylamine HPLC grade ($C_6H_{15}N$; 99%) and Tetrahydrofuran were obtained from Scharlau, Spain and Lobal Chemic Laboratory Reagent & Fine Chemicals, India, respectively. All the chemicals were analytical reagent (A.R) grade and were used as such. Milli-Q water was used for solution preparation. The required pH value was adjusted by 0.1 M NaOH or 0.1HCl.

2.2. Synthesis of crosslinked phosphorylated raw sawdust (RSD@P)

The RSD@P adsorbent was prepared using the following procedure [22]; for each 3 g of sawdust, a mixture of 10 ml of tetrahydrofuran (THF) and 5 ml of triethylamine (TEA) was added. Then, the mixture was cooled in an ice bath while adding 15 ml of phosphorus oxychloride dropwise. After that, the mixture was refluxed for 1 h. The obtained yield was repeatedly washed using pure hot water and dried at 70°C for 12 h.

2.3. Apparatus

The FTIR spectra of RSD@P before and after the dye adsorption were studied within the range 400–4,000 cm^{-1}, using a Fourier infrared spectrometer (FT-IR: Nicolet 6700, Thermo Scientific, USA). SEM-EDX analyses (JSM-5600LV JEOL, Japan) were used to check the surface images of the RSD@P. A UV Visible spectrophotometer Agilent Cary 60 Spectrophotometer (Agilent Technologies, USA) was used to determine the dye concentrations during adsorption process.

2.4. RSD@P surface charge determination

The point of zero charge (pHpzc) of RSD@P was determined using a zeta potential (z) analyzer (Nano Plus Series, Particulate Systems, USA). The z potential was measured as a function of pH at room temperature. The RSD@P sample was suspended in D.I. water and then sonicated during 10 min. The pHs of the dispersions were adjusted to the desired values with HCl (0.1 M) or NaOH (0.1 M). The dispersions were then allowed to settle during 24 h and the z potentials of supernatants were then measured.

2.5. Adsorption experiment

The dye adsorption assessment was achieved through batch experiments. The volume sample was 50 mL of known dye concentrations with the requested amount of the RSD@P. The mixture was magnetically stirred at 500 rpm for the requested time and temperature. The dye concentrations were determined at characteristic wavelength of 517 nm for safranin and 664 nm for methylene. It is worthy to refer that varying the pH of dye solution does not produce modification in the color of the dyes.

The adsorption capacity q_e ($mg.g^{-1}$) was calculated using the formula:

$$q_e = V\left(C_o - C_e\right)/W \tag{1}$$

where C_o ($mg.L^{-1}$) is the initial dye concentration, C_e ($mg.L^{-1}$) is the liquid concentration of the dye at equilibrium, V (L) is the volume of the solution and W (g) is the mass of RSD@P. The percent removal (%) of the dye can be calculated as follows:

$$\%\ \text{Removal} = \left[\left(C_o - C_e\right)/C_o\right]\times 100 \tag{2}$$

2.6. Desorption experiment

The study of the desorption process is a major concern from an environmental and commercial point of view. Currently, 0.01 g of RSD@P was used for the adsorption of 20 $mg.L^{-1}$ of each dye in 50 mL solution at a predetermined pH for a stirring time of 90 min at 500 rpm at 293 K. Batch desorption experiments at different desorption times were performed using different desorption agents with concentrations of 0.1 and 1 mole. Distilled water, acetic acid, HCl, HNO_3 and NaOH were investigated as desorption agents and desorption of dye was evaluated using the following equation:

$$\text{Desorption ratio} = \left(\text{Conc. of dye desorbed/ Conc. of dye adsorbed}\right)\times 100 \tag{3}$$

3. Results and discussion

The fully characterized phosphorylated saw dust adsorbent (RSD@P) by our group in the previous study [22] demonstrated that the surface of the RSD@P had pores and grooves. The determined BET surface area, pore volume and average particle size were 14.56 m^2/g, 0.0090 cm^3/g and 24 nm, respectively.

3.1. Adsorption studies

3.1.1. Effect of the initial pH

Overall, the adsorption process is affected by the pH solution, which controls both the adsorbent and dye charges. Fig. 2 shows the dependence of the safranin and methylene blue adsorption on the initial pH values of 3–13. Results show that the safranin removal percentage increases from 38% to 70% by increasing pH between 3 and 11. The uptake percentage of methylene blue also increases from 30% to 78% as increasing the pH value from 3 to 12. Therefore, adsorption of both cationic dyes by RSD@P significantly depended on pH values. In this context, the high percentage removal at alkaline pH values may refer to increasing the number of negatively charge deprotonated phosphate groups on RSD@P, which leads to enhancing the electrostatic attraction of both dye cations. At lower pH values, the competitive adsorption between excess H^+ ions and dye cations gives rise a decrease in dye adsorption. Results can be also explained in terms of zero point charge of the RSD@P (pHzpc = 3). Generally, at pH < pH_{ZPC}, the adsorbent surface becomes positive while it will be negatively charged at pH > pH_{ZPC}, Thus, the surface of RSD@P at pH above pHzpc (3) will acquire negative charge leading to an increase in the adsorption, as long as the dye molecules are positively charged. Similar observations have been illustrated on adsorption of such dyes using diverse adsorbents [21,23–26]. However, the net positive charge decreases with increasing pH value, it leads in the decrease in the repulsion between the adsorbed dyes and the dye thus, improving the adsorption removal. The greatest increase in adsorption above pH 9 can be attributed to reducing dye-dye repulsion of the charge similarity. This may result to interaction the positive charge of dye molecules with the pi –electron system of the adsorbed dye. Hence, the adsorbed dye molecules become as nuclei for more dye accumulation. Moreover, the adsorption of safranin may be enhanced due to the formation of H bonds between amino groups of safranin and function groups of RSD@P. The decrease in adsorption after the apt pH value may due to an increase of hydrated sodium as cation in the aqueous phase competing with dye for the adsorption sites on the RSD@P surface.

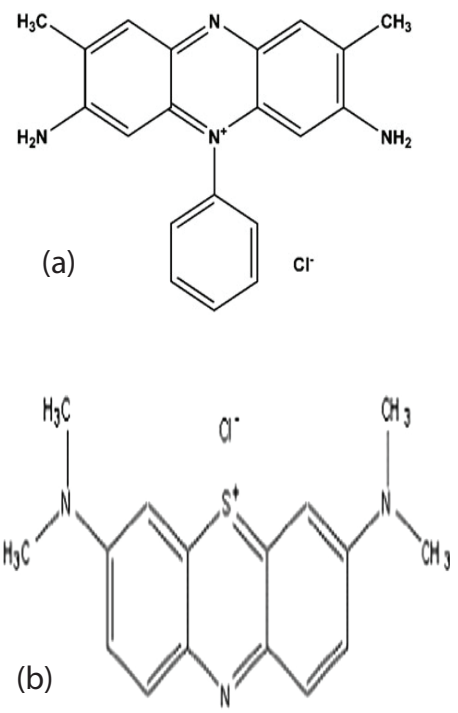

Fig. 1. Chemical structure of safranin (a) and methylene blue (b).

3.1.2. Effect of stirring time

Fig. 3 shows the effect of stirring time on the performance of dye adsorption at an optimal pH value and fixing all other experimental factors. The results show an increase of the adsorption percentage of safranin with increase in stirring time and it reaches to 82% at 90 min., and thereafter, the adsorption percentage displays about 5% more at increasing time up to 150 min. This observation may be attributed to difficult diffusion of aggregated dyes deeper to more micropores that already filled up [27] and hence, a little increase in adsorption is obtained after stirring time of 90 min. Therefore, at 90 min stirring time a steady-state

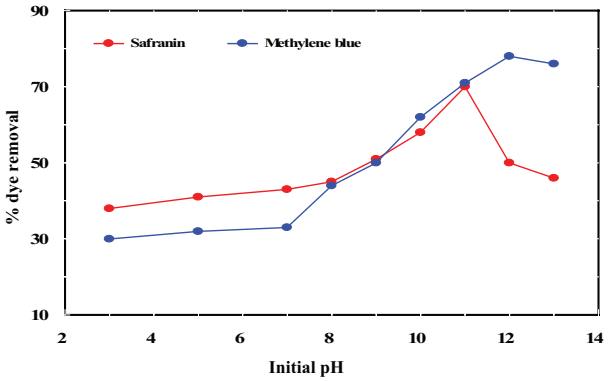

Fig. 2. Effect of the initial pH value on the percentage of safranin and methylene blue removal by RSD@P. Initial dye concentration = 20 mg/L, RSD@P amount = 0.01 g, sample volume = 50 mL, stirring time = 1 h at 500 rpm and temperature = 293 K.

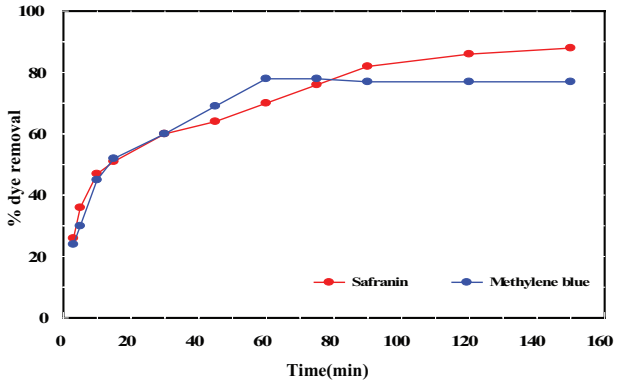

Fig. 3. Effect of stirring time on the removal of dyes onto 0.01g RSD@P using 20 mg/L as the safranin and methylene blue concentration. Volume solution = 50 mL, stirring rate = 500 rpm, temperature = 293 K and pH values of = 11 and 12 for the safranin and methylene blue, respectively.

approximation as quasi-equilibrium situation is assumed and this value is conducted for further experiment instead to 150 min. The percentage removal percentage of methylene blue also increases by increasing the stirring time reaching to equilibrium at 60 min. The significant increase of the dye adsorption percentage by increasing the stirring time may be due to an increase of the residential time provided for dye adsorption [28].

3.1.3. Effect of initial dye concentrations at different temperatures

The effect of initial dye concentration in the range of 10–150 mg/L on adsorption was investigated at 293, 303 and 318 K (Fig. 4). Results show that as increasing the initial dye concentrations the removal percentage of dye decreases at studied temperatures (safranin; 88%–14.5%, 90%–16.5%, 91.5%–18%; methylene blue; 83%–15%, 87%–18%, 89%–21% for 293, 303 and 318 K, respectively). Moreover, results show an improvement in the removal efficiency with increasing temperatures. The decrease in the dye percentage removal with increasing concentration may be referred to the decreasing of available active sides of RSD@P which become saturated at a definite concentration.

3.1.4. Effect of adsorbent dose

Fig. 5 shows the adsorption behavior of 20 mg/L of each aqueous dye solution as a function of the RSD@P dosage. The percentage dye removal increases on changing the adsorbent quantity from 0.001 to 0.03 g/50 mL. The percentage dye removal increases from 5% to 39% and 9.4% to 38%, with an increase in the RSD@P dose from 0.001 to 0.08 g for safranin and methylene blue, respectively. A sharp increase in removal is observed at 0.01 g of adsorbent, then an approximately 11% (safranin) and 13% (methylene blue) removal increase is obtained as adsorbent dose increases from 0.01 to 0.03 g. In general, a more adsorbent quantity leads to an increase in the displayed surface for adsorption, thus obtaining more available adsorption sites. A slight increase in adsorption after a 0.01 g adsorbent dose may be due to the adsorption sites being superimposed [29,30].

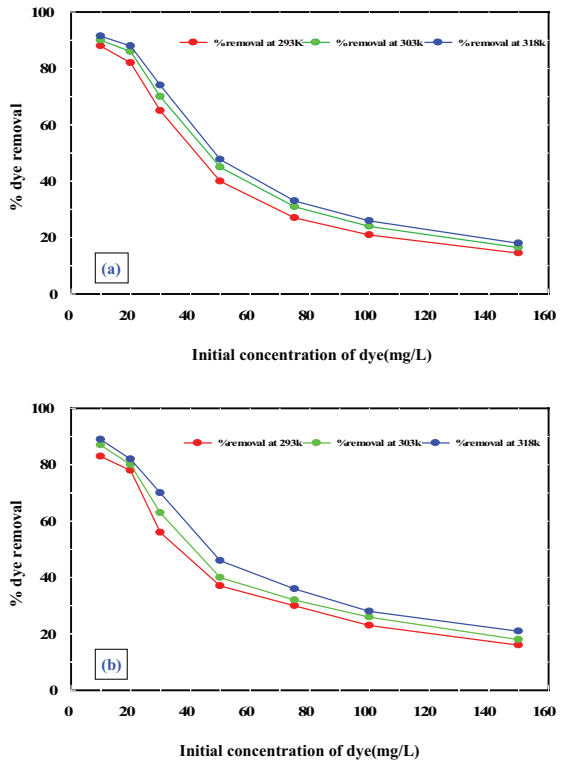

Fig. 4. Effect of dye concentration on the % removal using 0.01 g RSD@P at different temperatures. Volume solution = 50 mL, stirring rate = 500 rpm, pH = 11, stirring time = 90 min for safranin, (a) and pH = 12 and stirring time = 60 min for methylene blue, (b).

3.2. Adsorption kinetics

Four kinetic models are proposed to study both safranin and methylene blue adsorption. The study involved the treatment and fitting data of time-dependent adsorption to the linear form of four kinetic models, including pseudo-first and second-order models as well as Elovich and intra-particle diffusion equations (Table 1). The data show the results of the linear regressions of time vs. $\log(q_e-q_t)$ and t/q_t for the pseudo-first and second orders, respectively. They also refer to the linear relations between $1/\ln q_t$ against q_t for the Elovich model and $t^{1/2}$ as a result of q_t for the Weber–Morris intraparticle [16]. The most applicable model shows a closer correlation coefficient value (R^2) to 1 and the closeness the experimental adsorption capacity to the calculated value. Based on the comparison of R^2, the pseudo-second-order model is more significant and better for describing the adsorption of both dyes than the pseudo-first-order and Elovich models. Fig. 6 shows good agreement between the experimental data and the pseudo-second-order model (R^2 values of 0.9910 and 0.9977 for safranin and methylene blue, respectively). Overall, the pseudo-second-order model can be favorably fitted to both chemical and physical equilibriums [31,32]. This model involves two pathways; a fast one, which quickly attains equilibrium, while the other one is slower and takes a long time. As shown in Table 1, the pseudo second-order rate

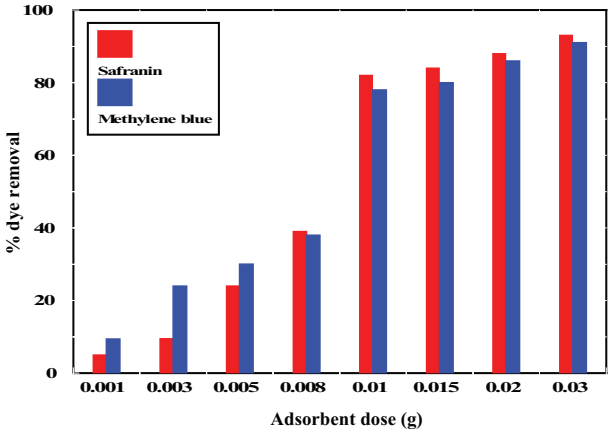

Fig. 5. Effect of RSD@P dosage on the % removal of dyes. Volume solution = 50 mL, stirring rate = 500 rpm, pH = 11, stirring time = 90 min for safranin, and pH = 12, and stirring time = 60 min for methylene blue.

Table 1
Correlation of some kinetic models with the experimental results of safranin and methylene blue adsorption by RSD@P at 293 K

Model	Linear form	Fitting results	
		Safranin	Methylene blue
Pseudo 1st order	$Log(q_e - q_t) = Log q_e - k_1 t/2.303$	$R^2 = 0.968$	$R^2 = 0.9749$
		$q_{cal.}$, mg.g^{-1} = 52.17	$q_{cal.}$, mg.g^{-1} = 55.02
		k_1, min^{-1} = 0.0269	k_1, min^{-1} = 0.0402
Pseudo 2nd order	$t/q_t = 1/k_2 q_e^2 + t/q_e$	R^2 = 0.9910	R^2 = 0.9977
		$q_{exp.}$, mg.g^{-1} = 88	$q_{exp.}$, mg.g^{-1} = 78
		$q_{cal.}$, mg.g^{-1} = 93.46	$q_{cal.}$, mg.g^{-1} = 82.64
		k_2, g.mg^{-1} min^{-1} = 8.24 × 10^{-4}	k_2, g.mg^{-1} min^{-1} = 1.53 × 10^{-3}
		h_o, mg.g^{-1} min^{-1} = 7.2	h_o, mg.g^{-1} min^{-1} = 10.48
Elovich model	$q_t = 1/\beta \ln(\alpha\ \beta) + 1/\beta \ln(t)$	R^2 = 0.8203	R^2 = 0.8774
		β, g.mg^{-1} = –0.0118	β, g.Mg^{-1} = –0.0117
		α, mg.g^{-1} min^{-1} = 4.75 × 10^{-3}	α, mg.g^{-1} min^{-1} = 4.61 × 10^{-3}
Weber and Morris	$q_t = k_b t^{1/2} + A$	R^2 = 0.9558	R^2 = 0.8286
Intraparticle		k_b, mg.g^{-1} min^{-1} = 5.624	k_b, , mg.g^{-1} min^{-1} = 5.137
		A, mg.g^{-1} = 25.405	A, mg.g^{-1} = 26.881

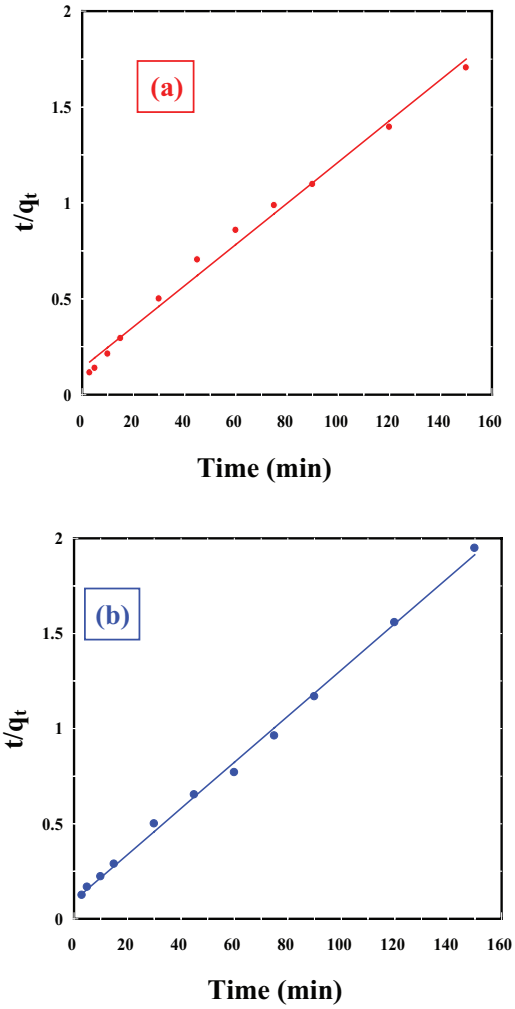

Fig. 6. Fitting the experimental results of safranin, (a) and methylene blue, (b) adsorption with pseudo-second-order at 293 K.

constant (k_2) is (8.24 × 10^{-4} and 1.53 × 10^{-3} g.mg^{-1} min^{-1}) at 293 K for safranin and methylene blue, respectively. The values of calculated equilibrium capacity ($q_{cal.}$; 93.46 and 82.64 mg.g^{-1}) are much closer to the experimental q values (88 and 78 mg.g^{-1}) for safranin and methylene blue, respectively. The results also show that the adsorption affinity ($h_o = k_2 q_e^2$) of methylene blue adsorption (h_o, mg g^{-1} min^{-1} = 10.48 mg g^{-1} min^{-1}) is greater than that of safranin (h_o, mg g^{-1} min^{-1} = 7.2 mg g^{-1} min^{-1}).

Although, the pseudo-first order model expressed a fairly high value of correlation coefficient (R^2 = 0.968 and 0.9749, for safranin and methylene blue, respectively), values of calculated q were not close to the experimental q as obtained from the pseudo-second-order model. The fitted experimental results to the Elovich model show lower values of correlation coefficient (R^2 = 0.8203 and 0.8774, for safranin and methylene blue, respectively) than that obtained from the pseudo-second-order model. The alpha values (initial sorption rate) predicted the initial sorption rate are much low (4.75 × 10^{-3} and 4.61 × 10^{-3} mg.g^{-1} min^{-1}, for safranin and methylene blue, respectively). Hence, the Elovich model is inadequate a kinetic model for the adsorption study.

Results of applying the intra-particle diffusion kinetic equation are shown in Fig. 7 and Table 1. The Figure show almost to three steps, meaning that the adsorption is dominated by several diffusion processes. The first and second portions indicate both the macro- and micro-pore diffusions, respectively [33,34]. Meanwhile, the three steps may also be attributed to the adsorption of the dyes to the boundary layer diffusion effect, a gradual equilibrium stage and a final equilibrium stage. The latter is slow due to the slow intra-particle diffusion when approaching the dye concentration's minimum [3]. The intra-particle diffusion rate constant (k_b) evaluated is 5.624 and 5.137 mg.g^{-1} min^{-1} for safranin and methylene blue, respectively. It was found that the first linear portion (not presented) did not pass the origin point and gave positive intercept values (2.26 and 3.16 for safranin and methylene blue, respectively), emphasizing the predominance of the boundary layer diffusion beside the pore one [34].

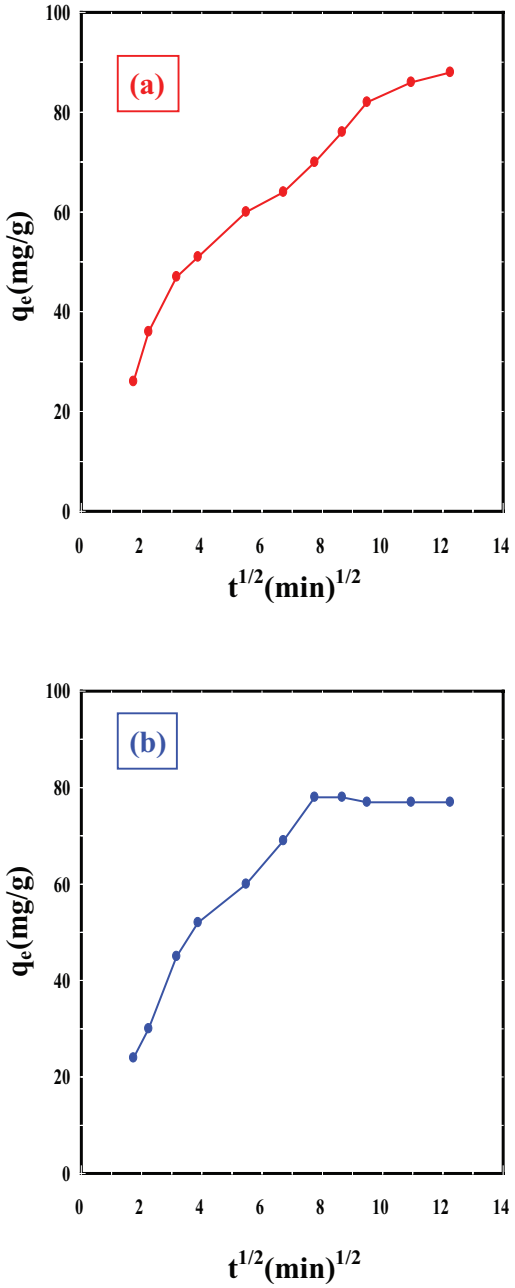

Fig. 7. Relation between q_e (mg/g) against the square root of stirring time $t^{1/2}$ (min)$^{1/2}$ of RSD@P at 293 K (safranin, (a) and methylene blue, (b)).

3.3. Adsorption isotherms

The study of adsorption equilibrium isotherms is very important for determining the sorbent capacity of current dyes and an adequate interpretation of the adsorption process. The obtained adsorption data at 293, 303 and 318 K were correlated with five adsorption isotherms; the Langmuir, Freundlich, Dubinin–Radushkevich, Temkin and Flory–Huggins isotherm models. The Langmuir isotherm is essentially applied to homogeneous adsorption and it describes the monolayer adsorption well. The linear form of this model is given by [35]:

$$C_e / q_e = 1 / q_m k_a + C_e / q_m \tag{4}$$

where C_e (mg.L^{-1}) is the dye's liquid concentration at equilibrium, q_e (mg g^{-1}) is the adsorption capacity, and q_m (mg. g^{-1}) and k_a (L. mg^{-1}) are the dye's maximum adsorption capacity at a complete monolayer formation on the surface and the affinity of the binding sites with the dye, respectively. On following this model, the experimental data should give a linear plot between C_e and C_e/q_e with a slope and intercept that can be used to determine q_m and k_a, respectively.

An important dimensionless equilibrium parameter of the Langmuir isotherm known as the separation factor (R_L) can be expressed as follows:

$$R_L = 1 / \left(1 + K_a C_o\right) \tag{5}$$

where k_a (L mg^{-1}) is the a constant obtained from the Langmuir equation and C_o (mg L^{-1}) is the initial dye concentration. In general, the value of R_L characterizes the nature of the dye adsorption. Accordingly, the adsorption process may be termed favorable, unfavorable, linear favorable or irreversible adsorption for R_L values between 0 and 1, greater than 1, or equal to 1 or 0, respectively [16,36].

The Freundlich isotherm is significant for treating multilayer heterogeneous adsorption with interaction between adsorbed species [3,37]. The linear form of the Freundlich model (Eq. (6)) illustrates the dependence of the adsorption capacity (q_e) on the equilibrium liquid adsorbate concentration (C_e).

$$\log q_e = \log K_F + 1 / n \log C_e \tag{6}$$

The values of K_F (mg.g^{-1}, adsorption capacity) and n (adsorption intensity) can be illustrated by the intercept and slope of the plot. The adsorption process can be inferred from the adsorption intensity factor (n) values. $N < 1$ adsorption is considered to be chemisorption, while $n > 1$ is physical adsorption and it becomes linear for $n = 1$ [38,39]. The Dubinin–Radushkevich isotherm model (Eqs. (7)–(9)) is used to differentiate between physical and chemical adsorption based on the mean energy of adsorption [40,41]:

$$\ln q_e = \ln q_m - \beta\varepsilon^2 \tag{7}$$

$$\varepsilon = RT\ln\left(1 + 1 / C_e\right) \tag{8}$$

$$E_{DR} = 1 / \left(2\beta\right)^{1/2} \tag{9}$$

where R is the gas constant (8.314 J.mol^{-1} K^{-1}), T is the temperature (K), C_o (mg L^{-1}) is the initial dye concentration and β is the isotherm constant. E_{DR} is the average adsorption energy, whose calculating value is also useful for classifying the adsorption process. E_{DR} values ranging from 8 to 16 kJ.mol^{-1} may refer to the adsorption's chemical nature, while values of $E_{DR} < 8$ kJ.mol^{-1} characterize physical adsorption [5,42].

Table 2
Fitting some adsorption isotherm models with the experimental data of safranin and methylene blue adsorption by RSD@P at different temperatures

Model	Dye	T/(K)		
		293	303	318
Langmuir	Safranin			
k_a (L.mg^{-1})		0.4656	0.4534	0.4002
q_m (mg.g^{-1})		109.218	124.715	135.899
R^2		0.9992	0.9995	0.9989
Freundlich				
K_f (mg.g^{-1})		55.169	58.9118	61.924
n		6.263	5.667	5.445
R^2		0.7442	0.7838	0.8042
Dubinin–Radushkevich				
q_m (mol.kg^{-1})		5.569×10^{-7}	6.23×10^{-7}	7.42×10^{-7}
β (mol^2.kJ^{-1})		1.31×10^{-3}	1.42×10^{-3}	1.47×10^{-3}
E (kJ.mol^{-1})		19.531	18.765	18.443
R^2		0.7891	0.8259	0.8446
Tempkin				
b_T (j.mol^{-1})		206.1191	174.6188	166.0719
a_T		121.2296	67.2838	56.3361
R^2		0.8185	0.8731	0.8967
Flory–Huggins				
n		–0.6285	–0.7068	–0.6341
k_f (L.M^{-1})		2.2926	2.4161	2.4943
ΔG° (kJ.mol)		–2.0211	–2.2222	–2.4165
R^2		0.8449	0.8412	0.8419
Langmuir	Methylene blue			
k_a (L.mg^{-1})		0.1852	0.1769	0.1694
q_m (mg.g^{-1})		123.457	138.89	158.730
R^2		0.9966	0.9948	0.9927
Freundlich				
K_f (mg.g^{-1})		45.991	49.037	52.312
n		11.289	4.438	4.117
R^2		0.8357	0.9081	0.9226
Dubinin–Radushkevich				
q_m (mol.kg^{-1})		6.574×10^{-7}	8.165×10^{-7}	9.909×10^{-7}
β (mol^2.kJ^{-1})		1.67×10^{-3}	1.82×10^{-3}	1.94×10^{-3}
E (kJ.mol^{-1})		17.303	16.575	16.054
R^2		0.8612	0.9305	0.9468
Tempkin				
b_T (j.mol^{-1})		158.8393	132.8185	118.3832
a_T		16.3952	10.6516	8.6353
R^2		0.8924	0.9616	0.9789
Flory–Huggins				
n		–0.9308	–0.7725	–0.6787
k_f (L.M^{-1})		2.2803	2.4278	2.5390
ΔG° (kJ.mol)		–2.0080	–2.2344	–2.4635
R^2		0.8609	0.8592	0.8620

The Temkin model considers the existence of interactions between adsorbate and adsorbent. It also assumes there is a linear decrease in the adsorption heat on increasing the surface coverage [32]. The linear form Temkin equation is:

$$q_e = RT/b_T Ln(a_T) + RT/b_T Ln(C_e) \quad (10)$$

where b_T (J. mol^{-1}) is the Temkin adsorption constant, a_T (L.g^{-1}) is the adsorption isotherm constant, R is the gas constant (8.314 J.mol^{-1} K^{-1}) and T is the temperature (K). Both the a_T and b_T values can be determined from the linear dependence of q_e on Ln (C_e).

The Flory–Huggins model is valuable for counting the degree of the adsorbate's surface coverage characteristics on the adsorbent and clears both the spontaneity and probability of the adsorption process [43]. The linear express of this isotherm has the following form:

$$\ln(\theta / C_o) = \ln K_{FH} + n\ln(1-\theta) \quad (11)$$

where $\theta = (1–C_e/C_o)$ refers to the degree of surface coverage, K_{FH} (L. mol^{-1}) is the equilibrium constant and n is the number of adsorbed dyes on the available sites.

Applying Eq. (11) gives a straight line with slope and intercept equal to n and ln k_{FH}, respectively. K_{FH} and the standard free energy change (ΔG^o) are related as follows:

$$K_{FH} = \exp(-\Delta G^\circ / RT) \quad (12)$$

The results of the correlated experimental data with the five adsorption models are presented in Table 2. With regard to the obtained correlation coefficients (R^2), the Langmuir adsorption model virtually displays higher values of R^2 than the others in both dye cases. The values of R^2 are 0.9992, 0.9995 and 0.9989 for the safranin dye; 0.9966, 0.9948 and 0.9927 for the methylene blue at 293, 303 and 318 K, respectively. The superiority of the Langmuir model suggests the homogeneous adsorption of both dyes on the RSD@P and the formation of a monolayer surface coverage. The Langmuir monolayer adsorption capacity calculated at 293, 303 and 318 K are 109.218, 124.715, 135.899 mg.g^{-1} and 123.457, 138.89, 158.730 mg.g^{-1} for safranin and methylene blue, respectively. The results in Table 2 also show the direct proportion of q_m with temperature, implying the endothermic nature of dye adsorption. Moreover, methylene blue displays higher adsorption capacities than safranin. This is attributed to the variation in chemical structure, molecular size and adsorption affinity referred to in the previous part. The calculated R_L values for different concentrations of safranin and methylene blue at the studied temperatures (293, 303 and 318 K) are 0.064, 0.065, 0.072 and 0.138, 0.143, 0.148, respectively. All the R_L values are within the 0–1 range; therefore, the adsorption of both dyes onto the RSD@P certainly undergoes a favorable process. Overall, increasing the temperature leads to an improvement in dye adsorption by changing the pore size and activating the RSD@P surface [16]. In addition to relying on R^2 value in figuring out the applicability of adsorption model, calculated some adsorption parameters are taken into account. Results

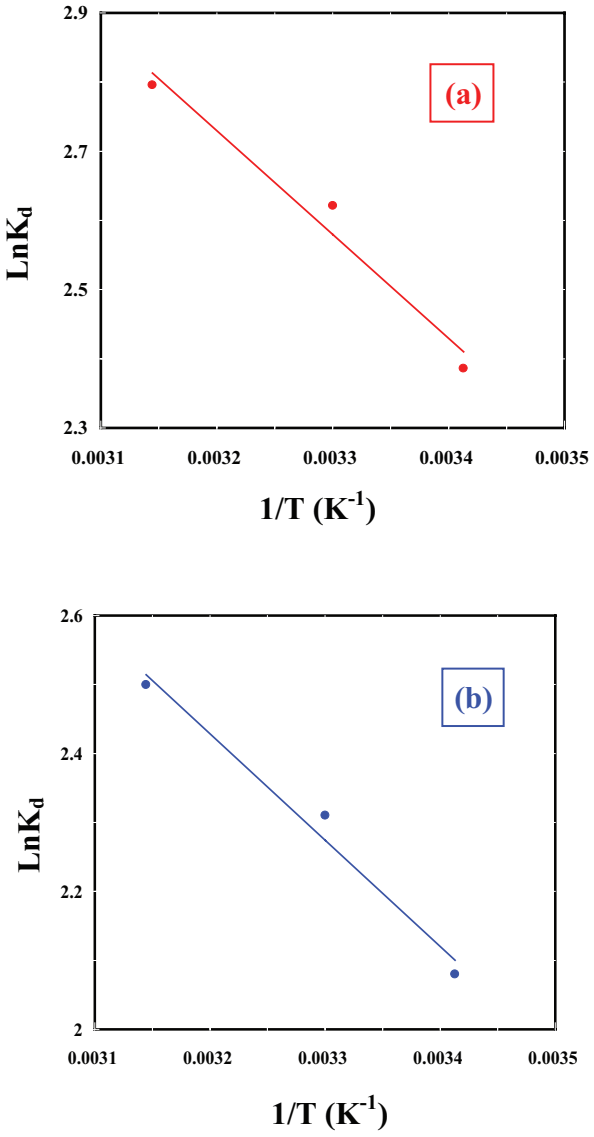

Fig. 8. Van't Hoff plots for the adsorption of safranin, (a) and methylene blue, (b) on the RSD@P.

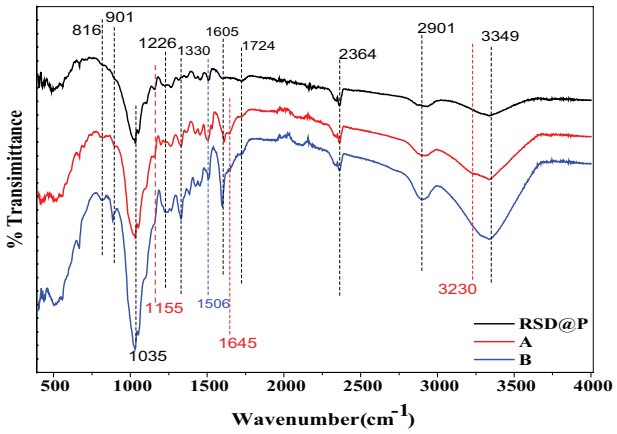

Fig. 9. FTIR of modified raw sawdust (RSD@P) before and after safranin (a) and methylene blue (b) adsorption.

of the calculated adsorption capacity (q_m) by Freundlich model for both dyes displayed lower values than those obtained by Langmuir adsorption model (Table 2). It has been found that values of activation energy (E) obtained from the Dubinin–Radushkevich isotherm model are greater than 8 kJ.mol^{-1} (Table 2). These values are contrary with the physical adsorption of these dyes on RSD@P. The obtained Temkin parameters (a_T and b_T) as shown in Table 2 are lower values suggesting its poor fit to the experimental data. However, the Flory–Huggins model displays fair fit with the experimental data (Table 2); the determined negative values of ΔG^o indicate the spontaneous nature of adsorption.

3.4. Adsorption thermodynamics

The determination of thermodynamic parameters is very important for the further investigation of adsorption behavior. Here, the free energy change (ΔG^o), enthalpy change (ΔH^o) and entropy change (ΔS^o) will be determined by the following thermodynamic laws and Van't Hoff Eqs. (13)–(15) using the obtained adsorption results of three different temperatures: 293, 303 and 318 K.

$$\Delta G° = -RT\ln K_d \tag{13}$$

$$\Delta G° = \Delta H° - T\Delta S° \tag{14}$$

$$\ln K_d = \Delta S° / R - \Delta H° / RT \tag{15}$$

where R is the gas constant (8.314 J.mol^{-1} K^{-1}), T is the temperature (K) and the K_d constant relates to the adsorption equilibrium or distribution coefficient. Its value can be obtained using the following equation [7,9,44,45]:

$$K_d = q_e / c_e \tag{16}$$

The listed values of ΔH^o and ΔS^o in Table 3 were calculated from the slope and intercept of the linear plots ln K_d against 1/T (Fig. 8). For both dyes, the ΔG^o values are negative and increase at increased temperature, indicating its favorability and spontaneity at the studied temperatures. The $\Delta H°$ values are found to be positive for both dyes, thus confirming the endothermic nature of adsorption. The type of adsorption can be classified according to the $\Delta H°$ values. Physical adsorption is characterized by $\Delta H°$

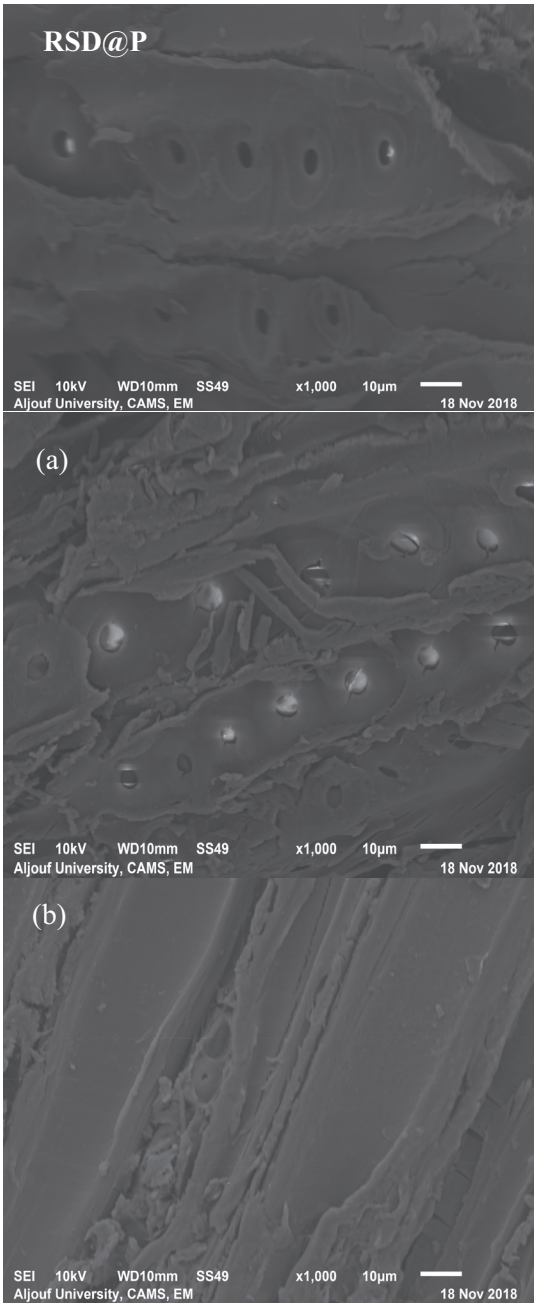

Fig. 10. SEM images of RSD@P before and after adsorption of safranin (a) and methylene blue (b).

Table 3
Thermodynamic data of safranin and methylene blue adsorption by RSD@P at different temperatures

Dye	Temperature (K)	K_d	ΔG^o (kj/mol)	ΔH^o (kj/mol)	ΔS^o (kj/mol)
Safranin	293	10.87	–5.81	12. 48	62.64
	303	13.76	–6.60		
	318	16.37	–7.39		
Methylene blue	293	8.00	–5.06	12. 83	61.24
	303	10.07	–5.82		
	318	12.18	–6.61		

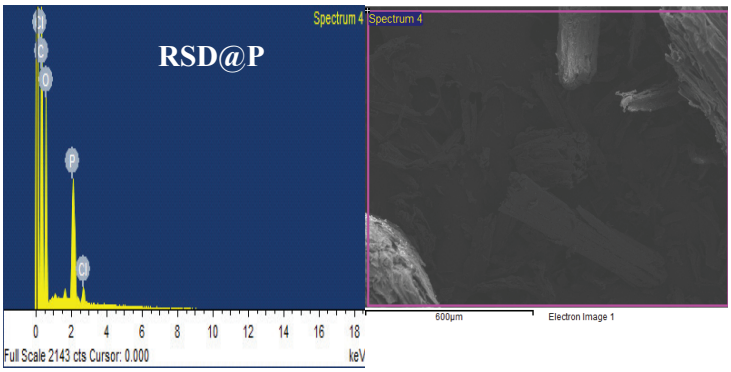

Element	Weight%	Atomic%
C K	60.05	68.75
O K	32.83	28.22
P K	8.81	4.14
Cl K	2.31	0.9

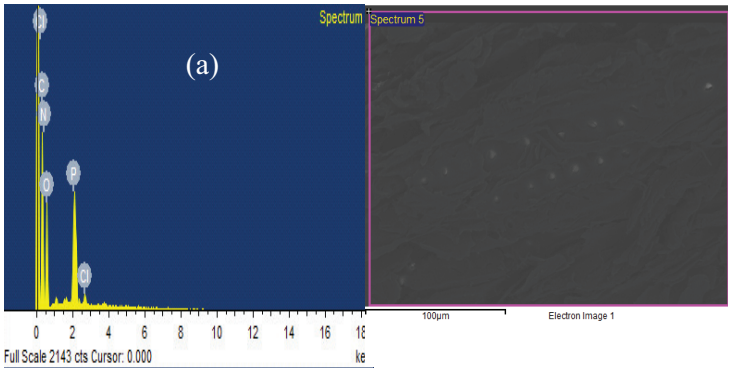

Element	Weight%	Atomic%
C K	54.40	64.46
N K	1.31	1.33
O K	32.59	28.99
P K	8.96	4.12
Cl K	2.74	1.10

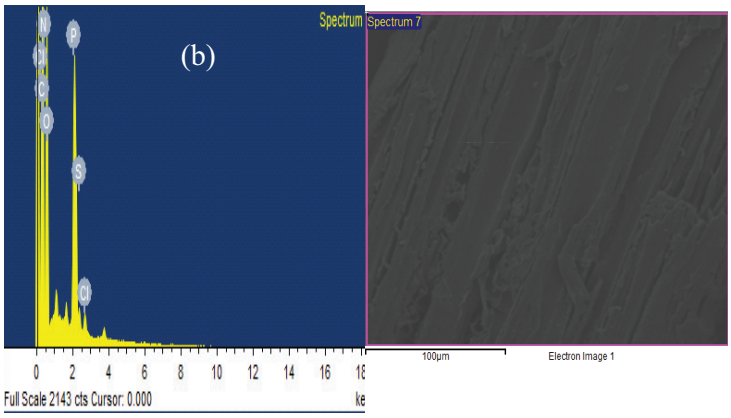

Element	Weight%	Atomic%
C K	52.80	64.68
N K	2.56	2.56
O K	36.85	32.32
P K	4.64	2.10
S K	1.84	0.81
Cl K	1.32	0.52

Fig. 11. SEM-EDX spectra of RSD@P before and after adsorption of safranin (a) and methylene blue (b).

values of 2.1–20.9 kJ. mol^{-1}, while $\Delta H°$ values between 80 and 200 kJ. mol^{-1} describe chemisorption. Accordingly, the current $\Delta H°$ values (12.48 and 12.82 kJ. mol^{-1} for safranin and methylene blue, respectively) certainly imply physical adsorption. Moreover, the positive $\Delta S°$ values indicate an increase in system randomness as there is more dye adsorption onto the RSD@P's solid surface of [3,16,19,44].

3.5. Dye desorption tests

The results generally show no appreciable increase in desorption efficiency on increasing the agent concentration. The final desorption percentages after 90 min are shown in Table 4. The results imply that the safranin desorption efficiency follows the order 0.1 M HCl > 0.1 M HNO3 > 0.1 M NaOH > CH_3COOH> DI H_2O. In case of methylene blue desorption, the same order is obtained with referring to convergent desorption results of acetic acid and distilled water. The highest desorption efficiencies of 24% and 15% with 0.1 M HCl are obtained for safranin and methylene blue, respectively. Results show the possibility of hydrolytic ruptures of possible links between dyes and adsorbent caused in neutral, acid and basic medium, being more efficient in acid medium, confirming the physical nature of both safranin and methylene blue dye's adsorption onto the RSD@P. Moreover, desorption of dyes by dilute mineral acids further indicates for the physisoprtion process [46]. However, the low desorption percentage may be attributed

to the available porosity and the binder nature of RSD@P which influence on retention ability of dyes and hence their fixation.

3.6. Proving the adsorption efficiency of safranin and methylene blue by RSD@P and in comparison with other sorbents

The removal percentage of safranin and methylene blue by 0.01 g of RSD@P using predetermined conditions was compared with that obtained using raw sawdust. The RSD@P shows 82% safranin removal at 90 min stirring time and 78% methylene blue removal at 60 min, while raw sawdust shows 44% and 41% removal for both dyes, respectively. This result certainly indicates the appropriateness of the current adsorbent for the removal of both dyes. The FTIR of the RSD@P before and after the adsorption of both dyes were also compared (Fig. 9). The FTIR spectrum for RSD@P shows a broad adsorption at 3,349 cm^{-1}, which can be assigned to the O–H stretching vibration mode of hydroxyl functional groups. The band observed at 2,901 cm^{-1} is attributed to the aliphatic –CH stretching vibrations. The peak at 1,724 cm^{-1} may be attributed to C=O stretching. The band observed at 1,605 cm^{-1} is due to either the C=O or the C=C aromatic ring stretching vibrations [23]. The band observed at 1,506 cm^{-1} offers the presence of C=O. The band observed at 1,330 cm^{-1} corresponds to the symmetric aliphatic C–H bending vibration of CH_3. The characteristic peak at 2,364 cm^{-1} is ascribed to P–H. Peaks at 1,233, 1155, 1035, 901, and 816 cm^{-1} refer to P=O and P–O groups [27,47–51]. After adsorption of dyes, a change in position and intensity of some absorption bands was observed. The observed peak of O–H was slightly altered to 3,342 cm^{-1} and became wide. The superimposed a weak shoulder at 3,220 cm^{-1} in spectrum (A), may be due to intermolecular hydrogen bonding between O–H and NH_2 of safranin dye. The presence of NH_2 is confirmed by N–H bending vibration at 1,645 cm^{-1}. The observed band at 1,605 cm^{-1} (C=O or the C=C aromatic ring stretching vibrations) shifted to 1,611 cm^{-1} (safranin) and 1,608 cm^{-1} (MB) with increasing the band intensity. The magnitude of corresponding band to symmetric aliphatic C–H bending vibration of CH_3 at 1,330 cm^{-1} was also increased. Moreover, peaks related to the P=O and P–O also displayed some changes, such as 1,233→1,197 (safranin), 1,204 (MB) and 1,155→1,161 (both dyes); while the intensity peak at 816, 901, 1035 cm^{-1} increased after adsorption. The peak at 1,226 cm^{-1} in the spectrum (B) shows the stretching vibration of C=S in methylene blue dye confirming its adsorption on the RSD@P surface.

Table 4
Desorption efficiency of safranin and methylene blue using several agents

Desorption agent	Dye	Efficiency desorption%
Distilled water		4.8
Acetic acid 0.1 M		7.3
HCl 0.1 M	Safranin	24
HNO_3 0.1 M		18
NaOH 0.1 M		10.8
Distilled water		4.2
Acetic acid 0.1 M		4.1
HCl 0.1 M	Methylene blue	15
HNO_3 0.1 M		11.5
NaOH 0.1 M		4.5

The SEM micrographs of the RSD@P before and after the adsorption of safranin and methylene blue are shown in Fig. 10. A clear difference between images can be observed. The surface of the RSD@P shows uneven spots where they were loaded by dyes after adsorption. The EDX analysis was also applied as an evident for dye adsorption (Fig. 11). Patterns and EDX analysis Tables of dye adsorption (Fig. 10(a), Fig 10(b)) show the appearance of nitrogen and sulfur peaks in addition to that already exist in RSD@P pattern. These results certainly confirm dye adsorption on RSD@P.

The RSD@P's maximum adsorption capacity q_m (mg/g) value was eventually reviewed with other studies conducted

Table 5
Comparison of safranin and methylene adsorption capacity with some other adsorbents

Sorbent	Dye	q_m (mg/g)	Reference
Calcined mussel shells	Safranin	154.34	[16]
Magnetic mesoporous clay		18.48	[19]
HDTMA-modified Spirulina sp.		54.05	[45]
RSD@P		109.22 (293 K)	[This work]
		124.715 (303 K)	
		135.899 (318 K)	
Biomass FA-geopolymer	Methylene blue	15.4	[8]
Raw kaolin		72.57	[18]
Zeolite		33.5	[52]
RSD@P		123.46 (293 K)	[This work]
		138.89 (303 K)	
		158.730 (318 K)	

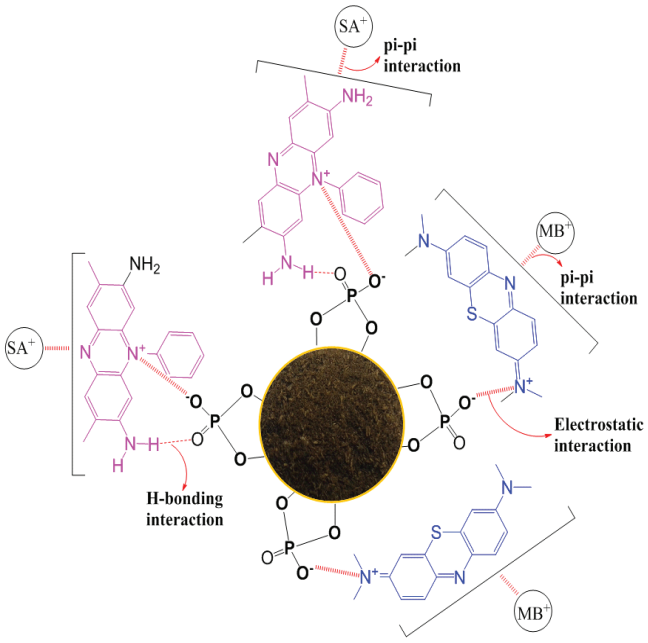

Fig. 12. Schematic adsorption mechanism of safranin and methylene blue by RSD@P.

(Table 5). The results of comparing the RSD@P's sorption capacity with some other sorbents show a relatively high sorption capacity compared with that of some of those reported. Therefore, the RSD@P appears to provide an effective surface for dye removal.

3.7. Adsorption mechanism

Fig. 12 shows the suggested adsorption mechanism for the removal of safranin and methylene blue by RSD@P. The adsorption mechanism involves electrostatic attraction between the dye and the adsorbent's surface function groups, formation of H bonds between amino groups of safranin and function groups of RSD@P, and the interaction between positive charges of dye molecules with the pi –electron system of the adsorbed dye.

4. Conclusions

Phosphorylated sawdust (RSD@P) was applied for safranin and methylene blue uptake from aqueous solutions. The study of all the experimental adsorption factors, as well as the kinetics, adsorption isotherm and thermodynamics, showed the effectiveness of removing dyes using RSD@P. The RSD@P showed superiority in the efficiency of dye removal rather than raw sawdust using the same dosage (0.01 g) and experimental conditions. It offered 82% safranin removal at 90 min stirring time and 78% methylene blue removal at 60 min, while raw sawdust showed 44% and 41% removal for both dyes, respectively. The adsorption process agreed with pseudo-second-order kinetics and the Langmuir model. With regard to the obtained thermodynamic parameters, the adsorption process could be characterized as a physical adsorption, spontaneous and endothermic reaction in nature.

References

[1] A.P. Lima Bazo, D.M.F. Salvadori, C.M. Rech, D.P. Oliveira, G.A. Umbuzeiro, Mutagenic and carcinogenic potential of a textile azo dye processing plant effluent that impacts a drinking water source, Mutat. Res., 626 (2007) 53–60.
[2] B. Mi-Hwa, O.I. Christianah, O. Se-Jin, K. Dong-Su, Removal of malachite green from aqueous solution using degreased coffee bean, J. Hazard. Mater., 176 (2010) 820–828.
[3] S. Kaur, S. Rani, R.K. Mahajan, M. Asif, V.K. Gupta, Synthesis and adsorption properties of mesoporous material for the removal of dye safranin: kinetics, equilibrium, and thermodynamics, J. Ind. Eng. Chem., 22 (2015) 19–27.
[4] S. Shariatia, M. Farajib, Y. Yamini, A.A. Rajabi, Fe_3O_4magnetic nanoparticles modified with sodium dodecyl sulfate for removal of safranin O dye from aqueous solutions, Desalination, 270 (2011) 160–165.
[5] S. Chowdhury, P. Saha, Adsorption kinetic modeling of safranin onto rice husk biomatrix using pseudo-first and pseudo-second order kinetic models: comparison of linear and non-linear methods. CLEAN. – Soil. Air. Water, 39 (2011) 274–282.
[6] A.K. Kushwaha, N. Gupta, M.C. Chattopadhyaya, Removal of cationic methylene blue and malachite green dyes from aqueous solution by waste materials of Daucus carota, J. Saudi. Chem. Soc., 18 (2014) 200–207.
[7] M.M. El-Moselhy, S.M. Kamal, Selective removal and preconcentration of methylene blue from polluted water using cation exchange polymeric material, Groundwater. Sustainable. Dev., 6 (2018) 6–13.
[8] R.M. Novais, G. Ascensao, D.M. Tobaldi, M.P. Seabra, J.A. Labrincha, Biomass fly ash geopolymer monoliths for effective methylene blue removal from wastewaters, J. Cleaner. Prod., 171 (2018) 783–794.
[9] L. Wang, J. Zhanga, A. Wang, Removal of methylene blue from aqueous solution using chitosan-g-poly (acrylic acid)/ montmorillonite super adsorbent nanocomposite, Colloids. Surf. A. Physicochem. Eng. Asp, 322 (2008) 47–53.
[10] A. Szygula, E. Guibal, M.A. Palacin, M. Ruiz, A.M. Sastre, Removal of an anionic dye (Acid Blue 92) by coagulation-flocculation using chitosan, J. Environ. Manage., 90 (2009) 2979–2986.
[11] E.A. DeLara, S.B. Damas, M.I.A. Miranda, M.I.I. Clar, Ultrafiltration technology with a ceramic membrane for reactive dye removal: optimization of membrane performance, J. Hazard. Mater., 209–210 (2012) 492–500.
[12] T.A. Saleh, V.K. Gupta, Photo-catalyzed degradation of hazardous dye methyl orange by use of a composite catalyst consisting of multi-walled carbon nanotubes and titanium dioxide, J. Colloid. Interface. Sci., 371 (2012) 101–106.
[13] C.R. Holkar, A.J. Jadhav, D.V. Pinjari, N.M. Mahamuni, A.B. Pandit, A critical review on textile wastewater treatments: possible approaches, J. Environ. Manage., 182 (2016) 351–366.
[14] C.H. Liua, J.S. Wua, H.C. Chiua, S.Y. Suena, K.H. Chub, Removal of anionic reactive dyes from water using anion exchange membranes as adsorbers, Water. Res., 41 (2007) 1491–1500.
[15] J. Zhang, Y. Zhou, M. Jiang, J. Li, J. Sheng, Removal of methylene blue from aqueous solution by adsorption on pyrophyllite, J. Mol. Liq., 209 (2015) 267–271.
[16] M. El Haddad, A. Regti, R. Slimani, S. Lazar, Assessment of the biosorption kinetic and thermodynamic for the removal of safranin dye from aqueous solutions using calcined mussel shells, J. Ind. Eng. Chem., 20 (2014) 717–724.
[17] M. Auta, B.H. Hameed, Chitosan-clay composite as highly effective and low-cost adsorbent for batch and fixed-bed adsorption of methylene blue, Chem. Eng. J., 237 (2014) 352–361.
[18] L. Mouni, L. Belkhiri, B. Jean-Claude, A. Bouzaza, A. Assadi, A. Tirri, F. Dahmoune, K. Madani, H. Remini, Removal of methylene blue from aqueous solutions by adsorption on kaolin: kinetic and equilibrium studies, Appl. Clay. Sci., 153 (2018) 38–45.
[19] M. Fayazi, D. Afzali, M.A. Taher, A. Mostafavi, V.K. Gupta, Removal of safranin dye from aqueous solution using magnetic mesoporous clay: optimization study, J. Mol. Liq., 212 (2015) 675–685.

[20] F.S. Teodoro, M.M.C. Elias, G.M.D. Ferreira, O.F.H. Adarme, R.M.L. Savedra, M.F. Siqueira, L.H.M. da Silva, L.F. Gil, L.V.A. Gurgel, Synthesis and application of a new carboxylated cellulose derivative. Part III: removal of auramine-O and safranin-T from mono- and bi-component spiked aqueous solutions, J. Colloid. Interface. Sci., 512 (2018) 575–590.
[21] P.S. Kumar, J. Pavithra, S. Suriya, M. Ramesh, K.A. Kumar, Sargassum wightii, a marine alga is the source for the production of algal oil, bio-oil, and application in the dye wastewater treatment, Desal. Wat. Treat., 55 (2015) 1342–1358.
[22] M.S. Alhumaimess, I.H. Alsohaimi., A.A. Alqadami, M.M. Kamel, Mu. Naushad, T. Ahamad, H. Alshammari, Synthesis of phosphorylated raw sawdust for the removal of toxic metal ions from aqueous medium: adsorption mechanism for clean approach, J. Sol-Gel. Sci. Technol., 89 (2019) 602–615
[23] P.S. Kumar, P.S.A. Fernando, R.T. Ahmed, R. Srinath, M. Priyadharshini, A.M. Vignesh, A. Thanjiappan, Effect of temperature on the adsorption of methylene blue dye onto sulfuric acid- treated orange peel, Chem. Eng. Comm., 201 (2014) 1526–1547.
[24] S. Suganya, P. Senthil Kumar, A. Saravanan, P. Sundar Rajan, C. Ravikumar, Computation of adsorption parameters for the removal of dye from wastewater by microwave assisted sawdust: theoretical and experimental analysis, Environ. Toxicol. Pharmacol., 50 (2017) 45–57.
[25] P.S. Kumar, R.V. Abhinaya, K.G. Lashmi, V. Arthi, R. Pavithra, V. Sathyaselvabala, S.D. Kirupha, S. Sivanesan, Adsorption of methylene blue dye from aqueous solution by agricultural waste: equilibrium, thermodynamics, kinetics, mechanism and process design, Colloid. J., 73 (2011) 647–657.
[26] K.O. Adebowale1, B.I. Olu-Owolabi1, E.C. Chigbundu, Removal of safranin-O from aqueous solution by adsorption onto kaolinite clay, J. Encap. Ads. Sci., 4 (2014) 89–104.
[27] P.S. Kumar, S. Ramalingam, C. Senthamarai, M. Niranjanaa, P. Vijayalakshmi, S. Sivanesan, Adsorption of dye from aqueous solution by cashew nut shell: studies on equilibrium isotherm, kinetics and thermodynamics of interactions, Desalination, 261 (2010) 52–60.
[28] P.S. Kumar, R. Sivaranjanee, U. Vinothini, M. Raghavi, K. Rajasekar, K. Ramakrishnan, Adsorption of dye onto raw and surface modified tamarind seeds: isotherms, process design, kinetics and mechanism, Desal. Wat. Treat., 52 (2014) 2620–2633.
[29] A.A. Inyinbor, F.A. Adekola, G.A. Olatunji, Kinetics, isotherms and thermodynamic modeling of liquid phase adsorption of Rhodamine B dye onto *Raphia hookerie* fruit epicarp, Water Resour. Ind, 15 (2016) 14–27.
[30] M.S. Kini, M.B. Saidutta, V.R.C. Murty, V.S. Kadoli, Adsorption of basic dye from aqueous solution using HCl treated saw dust (*Lagerstroemia microcarpa*): kinetic, modeling of equilibrium, thermodynamic, INDIA, Int. Res. J. Environment Sci., 2 (2013) 6–16.
[31] Y. Khambhaty, K., S. Basha, B. Jha, Kinetics, equilibrium and thermodynamic studies on biosorption of hexavalent chromium by dead fungal biomass of marine Aspergillus niger, Chem. Eng. J.,145 (2009) 489–495.
[32] R. Khosravi, G. Moussavi, M.T. Ghaneian, M.H. Ehrampoush, B. Barikbin, A.A. Ebrahimi, G. Sharifzadeh, Chromium adsorption from aqueous solution using novel green nanocomposite: adsorbent characterization, isotherm, kinetic andthermodynamic investigation, J. Mol. Liq., 256 (2018) 163–174.
[33] W.H. Cheung, Y.S. Szeto, G. McKay, Intraparticle diffusion processes during acid dye adsorption onto chitosan, Bioresour. Technol., 98 (2007) 2897–2904.
[34] K. Biswas, K. Gupta, U.C. Ghosh, Adsorption of fluoride by hydrous iron(III)–tin(IV) bimetal mixed oxide from the aqueous solutions, Chem. Eng. J., 149 (2009) 196–206.
[35] B. Hadi, T. Saeed, Treatment of nickel ions from contaminated water by magnetite based nanocomposite adsorbents: effects of thermodynamic and kinetic parameters and modeling with Langmuir and Freundlich isotherms, Proc. Saf. Environ. Prot., 109 (2017) 465–477.
[36] L. Yeon-Su, K. Jin-Hyun, Isotherm, kinetic and thermodynamic studies on the adsorption of 13-dehydroxybaccatin III from Taxus chinensis onto Sylopute, J. Chem. Thermodyn., 115 (2017) 261–268.
[37] B. Shuangyou, L. Kai, N. Ping, P. Jinhui, J. Xu, T. Lihong, Highly effective removal of mercury and lead ions from wastewater by mercaptoamine-functionalised silica-coated magnetic nano-adsorbents: behaviours and mechanisms,. Appl. Surf. Sci., 393 (2017) 457–466.
[38] M. Said, R.L. Machunda, Defluoridation of water supplies using coconut shells activated carbon: batch studies, Int. J. Sci. Res., 3 (2014) 2327–2331.
[39] C. Pongener, P.C. Bhomick, A. Supong, M. Baruah, U.B. Sinha, D. Sinha, Adsorption of fluoride onto activated carbon synthesized from Manihot esculenta biomass-Equilibrium, kinetic and thermodynamic studies, J. Environ. Chem. Eng., 6 (2018) 2382–2389.
[40] A. Ozcan, E.M. Oncu, S. Ozcan, Kinetics, isotherm and thermodynamic studies of adsorption of acid blue 193 from aqueous solutions onto natural sepiolite, Colloids. Surf. A. Physicochem. Eng. Aspects, 277 (2006) 90–97.
[41] K.Y. Foo, B.H. Hameed, Insights into the modeling of adsorption isotherm systems, Chem. Eng. J., 156 (2010) 2–10.
[42] A.Q. Selim, E.A. Mohamed, M. Mobarak, A.M. Zayed, M.K. Seliem, S. Komarneni, Cr(VI) uptake by a composite of processed diatomite with MCM-41: isotherm, kinetic and thermodynamic studies, Microporous. Mesoporous. Mater., 260 (2018) 84–92.
[43] M. Horsfall, A.I. Spiff, Equilibrium sorption study of Al^{3+}, Co^{2+} and Ag^{2+} in aqueous solutions by fluted pumpkin (Telfairia occidentalis HOOK) waste biomass, Acta. Chim. Slov., 52 (2005) 174–181.
[44] B. Yu, X. Zhang, J. Xie, R. Wu, X. Liu, H. Li, F. Chen, H. Yang, Z. Ming, S. T. Yang, Magnetic graphene sponge for the removal of methylene blue, Appl. Surf. Sci., 351 (2015) 765–771
[45] U.A. Guler, M. Ersan, E. Tuncel, F. Dügenci, Mono and simultaneous removal of crystal violet and safranin dyes from aqueous solutions by HDTMA-modified *Spirulina sp*., Proc. Saf. Environ. Prot., 99 (2016) 194–206.
[46] M. Hema, P.M.D. Prasath, S. Arivoli, Adsorption of malachite green onto carbon prepared from borassus bark, Arab. J. Sci. Eng., 34 (2009) 31–42.
[47] Y. Jin, G. Huang, D. Han, P. Song, W. Tang, J. Bao, R. Li, Y. Liu, Functionalizing graphene decorated with phosphorus-nitrogen containing dendrimer for high-performance polymer nanocomposites, Composites: Part A, 86 (2016) 9–18.
[48] F. Sun, T. Yu, C. Hu, Y. Li, Influence of functionalized graphene by grafted phosphorus containing flame retardant on the flammability of carbon fiber/epoxy resin (CF/ER) composite, Compos. Sci. Technol., 136 (2016) 76–84.
[49] W. Wang, Y. Kan, H. Pan, Y. Pan, B. Li, K.M. Liew, Y. Hu, Phosphorylated cellulose applied for the exfoliation of LDH: an advanced reinforcement for polyvinyl alcohol, Composites: Part A, 94 (2017) 170–177.
[50] S. Majumdar, B. Adhikari, Polyvinyl alcohol–cellulose composite: a taste sensing material, Bull. Mater. Sci., 28 (2005) 703–712.
[51] J-D. Zuo, S-M. Liu, Q. Sheng, Synthesis and application in polypropylene of a novel of phosphorus-containing intumescent flame retardant, Molecules, 15 (2010) 7593–7602.
[52] K. Rida, S. Bouraoui, S. Hadnine, Adsorption of methylene blue from aqueous solution by kaolin and zeolite, Appl. Clay. Sci., 83–84 (2013) 99–105.